AIP | The Journal of Chemical Physics

Photodissociation dynamics of the methyl perthiyl radical at 248 and 193 nm using fast-beam photofragment translational spectroscopy

Aaron W. Harrison, Mikhail Ryazanov, Erin N. Sullivan, and Daniel M. Neumark

Citation: The Journal of Chemical Physics **145**, 024305 (2016); doi: 10.1063/1.4955195
View online: http://dx.doi.org/10.1063/1.4955195
View Table of Contents: http://scitation.aip.org/content/aip/journal/jcp/145/2?ver=pdfcov
Published by the AIP Publishing

Photodissociation dynamics of the methyl perthiyl radical at 248 and 193 nm using fast-beam photofragment translational spectroscopy

Aaron W. Harrison,[a] Mikhail Ryazanov,[b] Erin N. Sullivan, and Daniel M. Neumark[c]
Department of Chemistry, University of California, Berkeley, California 94720, USA and Chemical Sciences Division, Lawrence Berkeley National Laboratory, Berkeley, California 94720, USA

(Received 9 May 2016; accepted 21 June 2016; published online 12 July 2016)

The photodissociation dynamics of the methyl perthiyl radical (CH_3SS) have been investigated using fast-beam coincidence translational spectroscopy. Methyl perthiyl radicals were produced by photodetachment of the CH_3SS^- anion followed by photodissociation at 248 nm (5.0 eV) and 193 nm (6.4 eV). Photofragment mass distributions and translational energy distributions were measured at each dissociation wavelength. Experimental results show S atom loss as the dominant (96%) dissociation channel at 248 nm with a near parallel, anisotropic angular distribution and translational energy peaking near the maximal energy available to ground state CH_3S and S fragments, indicating that the dissociation occurs along a repulsive excited state. At 193 nm, S atom loss remains the major fragmentation channel, although S_2 loss becomes more competitive and constitutes 32% of the fragmentation. The translational energy distributions for both channels are very broad at this wavelength, suggesting the formation of the S_2 and S atom products in several excited electronic states. *Published by AIP Publishing.* [http://dx.doi.org/10.1063/1.4955195]

I. INTRODUCTION

The disulfide bond is a common bonding motif found in a variety of contexts in nature. In protein chemistry, disulfide bonds between cysteine residues have a profound impact on the secondary structure of the protein that ultimately determines much of its functionality.[1] In addition, simple disulfides like dimethyl disulfide (DMDS) are common in seawater and in the atmosphere and make an important contribution to the global sulfur cycle.[2,3] The oxidation of these molecules in the combustion or in the atmosphere contributes to SO_x pollutants that can have adverse health effects and lead to acid rain. The corresponding open-shell disulfide radicals are of interest as possible intermediates in disulfide chemistry. Disulfide radicals are sulfur analogues of peroxy radicals, which are key intermediates in the oxidation of organic molecules,[4] but considerably less is known about their spectroscopy and primary chemical and photochemical pathways. In this article, we investigate the photodissociation dynamics of the methyl perthiyl radical (CH_3SS) at 248 and 193 nm.

Previous studies on the ultraviolet photodissociation of DMDS have found excited methyl perthiyl as one of the primary photoproducts at 195 nm[5] and 193 nm[6,7] that consequently decays to produce S_2. However, S_2 production has also been attributed to absorption of an additional photon by the nascent CH_3SS fragment.[8] At 248 nm, Lee *et al.*[6] found that DMDS photodissociation occurs through impulsive S–S bond cleavage, producing an anisotropic distribution of high translational energy CH_3S fragments that was ascribed to a $\sigma^*_{ss} \leftarrow n_s$ transition in DMDS.

There have also been a few spectroscopic studies of the methyl perthiyl radical itself. The electron affinity (EA) of CH_3SS was determined by Moran and Ellison[9] using anion photoelectron spectroscopy. The photoionization of methyl perthiyl has also been carried out.[10,11] Theoretical studies have been reported on the possible isomers of singly charged (±) and neutral CH_3SS[12] as well as the low-lying excited states of the CH_3SS and its cation.[13]

At the photodissociation wavelengths used here, three product channels are accessible,

$$CH_3SS \rightarrow CH_2S + SH \quad D_0 = 1.99\ \text{eV} \quad (1)$$

$$\rightarrow CH_3 + S_2 \quad D_0 = 2.11\ \text{eV} \quad (2)$$

$$\rightarrow CH_3S + S \quad D_0 = 3.45\ \text{eV}. \quad (3)$$

All energies are for the formation of products in their ground electronic states.[10,14–16]

The present work is motivated, in part, by a previous study on the photodissociation dynamics of methyl perthiyl carried out on a complementary molecular beam photofragment translational spectroscopy instrument in our research group.[17] In that study, flash pyrolysis of DMDS precursor was used to generate the methyl perthiyl radical prior to photodissociation at 248 nm; scattered product was detected with a rotatable mass spectrometer. These results showed evidence for S_2 and SH product formation from channels (2) and (1), respectively, but products from S–S bond cleavage were not observed. However, there was significant contamination from the DMDS precursor. Preliminary results described in the present paper motivated a re-investigation of CH_3SS photodissociation on the molecular beam instrument,[18] using

[a]Current address: School of Chemistry, University of New South Wales-Kensington, Sydney, NSW 2052, Australia.
[b]Current address: JILA, 440 University Ave., Boulder, Colorado 80309, USA.
[c]Author to whom correspondence should be addressed. Electronic mail: dneumark@berkeley.edu

dimethyl trisulfide as the precursor in the flash pyrolysis source, as its dissociation energy to CH_3SS is lower than that of DMDS. Moreover, an electron-impact ionizer with tunable electron energy was installed in the mass spectrometer to facilitate optimization of the source conditions to produce CH_3SS. The new results showed that at 248 nm, channel (3) dominated with a small contribution from channel (2). In addition, when the new ionizer was used to characterize the flash pyrolysis source using DMDS as a precursor, there appeared to be little or no CH_3SS produced under the conditions used in our original study, rendering those results suspect.

Herein, we report results on the photodissociation of the methyl perthiyl radical by fast beam coincident photofragment translational spectroscopy.[19] The radicals are prepared by near-threshold photodetachment of the corresponding anion, CH_3SS^-, and then photodissociated at 248 and 193 nm. We obtain translational energy and angular distributions of photofragments, $P(E_T,\theta)$, as well as branching ratios for the competing dissociation channels. These results show that at 248 nm, there is nearly exclusive formation of ground-state $CH_3S + S$ photofragments with the corresponding translational energy distribution peaking near the maximal available energy. At 193 nm, S loss remains the dominant channel (68%), with the remainder comprising S_2 loss. Translational energy distributions for both dissociation channels suggest the formation of products in a variety of excited electronic states.

II. EXPERIMENTAL METHODS

The fast-beam coincidence translational spectrometer used in this study has been described in detail previously.[20,21] The instrument has recently been modified to enable photoelectron detection and energy analysis (see below); its current configuration is shown in Figure 1. In this experiment, a fast beam of mass-selected CH_3SS^- anions is generated and photodetached to make a fast beam of methyl perthiyl radicals. The radicals are dissociated by a second laser, and the neutral fragments are detected in coincidence,

$$CH_3SS^- \xrightarrow{h\nu_1} CH_3SS \xrightarrow{h\nu_2} \text{fragments}. \quad (4)$$

Here, a mixture of ~0.1% of dimethyl disulfide (DMDS) in argon at 6.2 bars (75 psig) is expanded into the vacuum chamber through a pulsed molecular-beam valve equipped with a DC discharge source[22] to produce CH_3SS^- anions. To make CD_3SS^- anions, d_6-dimethyl sulfide was used. The anions are accelerated to a beam energy of 8 keV and mass-selected using a Bakker-type mass spectrometer[23,24] that imparts negligible kinetic energy spread to the ion beam. Mass-selected anions are then photodetached at 698 nm (1.777 eV) with a Nd:YAG-pumped dye laser (Litron LPY742-100 and Radiant Dyes NarrowScan). This detachment energy is chosen to lie only slightly above the electron affinity of methyl perthiyl, 1.757 eV (1.748 eV for CD_3SS),[9] in order to minimize the production of vibrationally excited radicals. Undetached anions are deflected out of the beam, leaving behind a fast beam of neutral methyl perthiyl radicals. This neutral packet is then intersected by a UV pulse from an excimer laser (GAM EX-50F) at 248 nm (5.0 eV) or 193 nm (6.4 eV). The two lasers and pulsed beam valve operate at a repetition rate of 100 Hz. Photofragments from dissociated radicals recoil off the beam axis and strike a time- and position-sensitive (TPS) detector located 1.36 m downstream from the photodissociation region, while undissociated radicals are flagged by a beam block (4 mm radius) in front of the detector.

For coincident TPS measurements of the photofragments, a Roentdek Hex80 delay-line anode detector[25] is used. The Roentdek hexanode and the principles underlying delay-line detection have been described in detail elsewhere.[25–27] The position and time resolution of this setup are estimated to be 100 ps and 100 μm, respectively.[28,29] Based on calibration experiments using the predissociation from the $B^3\Sigma_u^-$ state of

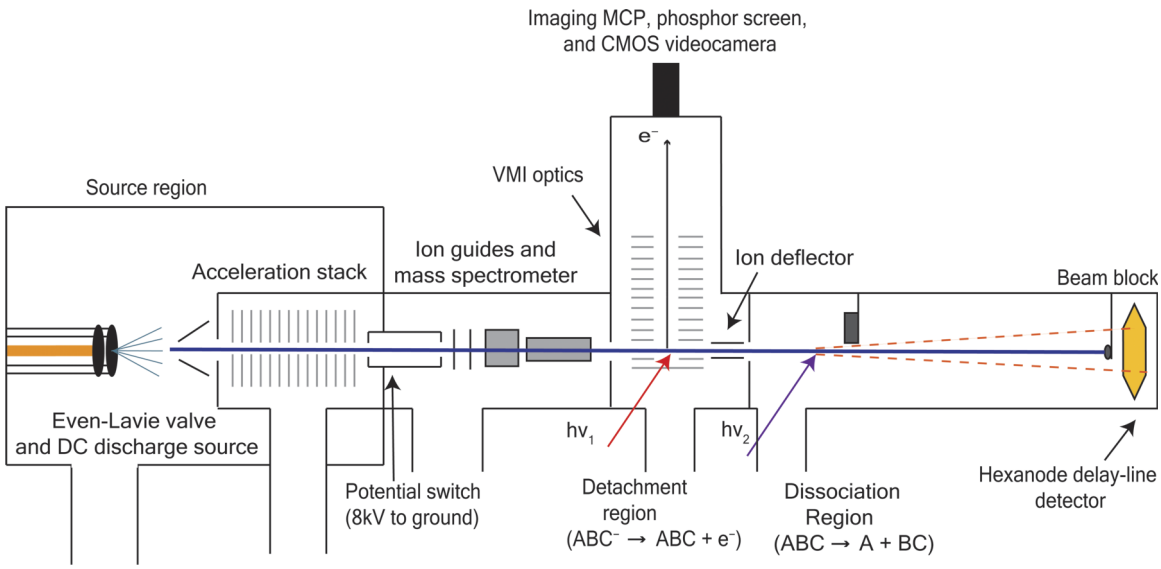

FIG. 1. Schematic of fast-beam photofragment translational spectrometer with orthogonal, velocity-map imaging (VMI) setup for photoelectron detection.

O_2, the kinetic energy resolution ($\Delta E/E$) is measured to be ~0.8%.[30]

With this instrument, the hit positions and arrival times at the detector are determined for both photofragments from each dissociation event, thereby yielding the translational energy release, scattering angle, and photofragment mass ratio for each event. From these, we can construct the translational energy and angular distribution, $P(E_T, \theta)$, given by the following uncoupled relation:

$$P(E_T, \theta) = P(E_T) \cdot [1 + \beta(E_T) P_2(\cos\theta)], \quad (5)$$

where β is the energy-dependent anisotropy parameter and P_2 is the 2nd-order Legendre polynomial.[31] For this experiment, θ is defined as the angle between the dissociation recoil axis and the laser propagation direction, as the unpolarized output from our GAM excimer laser was used for photodissociation. In this case, β takes on the values between −1 for parallel and 1/2 for perpendicular transitions, respectively, corresponding to the β-parameter values for the linearly polarized light multiplied by −1/2.

The presence of the beam block and the finite radius of the detector lead to lower detection efficiency and larger uncertainty in the measured intensity for events with very low and high translational energies; this effect depends on the photofragment recoil angle as well. To account for these effects, the raw translational energy distributions are adjusted with a detector acceptance function (DAF)[19] calculated from the known geometrical and kinematic parameters of the setup. The $P(E_T, \theta)$ distributions and branching ratios presented here have all been corrected using the DAF.

A. Photoelectron spectrometer

In this experiment, anions are typically photodetached at photon energies just above the electron affinity in order to minimize vibrational energy of the resulting radical. However, if the anion is itself vibrationally excited, then this energy will generally be transferred to the radical. In order to be able to monitor (and hopefully minimize) the extent of anion vibrational excitation, we have recently installed a velocity-map imaging (VMI) photoelectron spectrometer in the detachment region of our instrument to characterize the internal energy distribution of the neutral radicals prior to photodissociation. A cross-sectional view of the electron-optical assembly is shown in the supplementary material.[32] The multi-plate design was extensively optimized based on simulations of electron trajectories, similar to the approach used previously in designing a high-resolution photofragment imaging apparatus.[33] Details of the design, optimization procedure, and performance are given in the supplementary material.[32]

For the VMI photoelectron spectrometer not to interfere with the fast-beam operation, it was installed in an orthogonal configuration, with the VMI axis perpendicular to the ion beam. This has two important consequences. First, the detached photoelectrons inherit from the fast parent ion beam a substantial drift velocity that is comparable to their own ejection velocities and leads to a significant shift of the image on the detector. Therefore, the electron optics have to perform well for off-center images, and the VMI parameters, especially for imaging slow (in the ion frame of reference) electrons, might be affected. Second, since the detachment region is located inside the electron optics, the ion beam is also affected by the VMI fields, possibly reducing its overlap with the detachment laser beam. To counteract that effect, the distance traveled by the ion beam inside the VMI field is minimized, and deflector plates with an opposing field are installed in front of the electron optics.

The overall energy resolution of the spectrometer, as tested on photodetachment of O^- and OH^- (see supplementary material[32]), is around 0.3% even for relatively slow electrons (kinetic energy of ~0.25 eV). This performance is comparable to the highest-resolution negative-ion VMI spectrometers previously reported.[34,35]

III. EXPERIMENTAL RESULTS

A. Anion photoelectron spectrum (PES) of CH_3SS^-

The anion photoelectron spectra (PES) of both CH_3SS^- and CD_3SS^- were measured previously, yielding electron affinities (EAs) of 1.757 eV and 1.748 eV for the corresponding radicals.[9] To minimize the amount of excess energy imparted to the neutral radical in the detachment step, the photodetachment laser was tuned to λ = 698 nm (1.777 eV), just above the EA. The resulting PES for CH_3SS^- is shown in Figure 2, with spectroscopic features labelled A–E. The major feature A at 0.020 eV in the PES corresponds to the vibrational origin (0-0) transition. The additional peaks in the spectrum (B-E) are due to transitions from vibrationally excited anions created in the discharge source. To aid in the assignment of this spectrum, we conducted Franck–Condon (FC) simulations (discussed in Sec. IV A) using the calculated anion and neutral frequencies (Table I) and the program ezSpectrum.[36] The results of the FC simulations at a vibrational temperature of 200 K are shown in red in Figure 2.

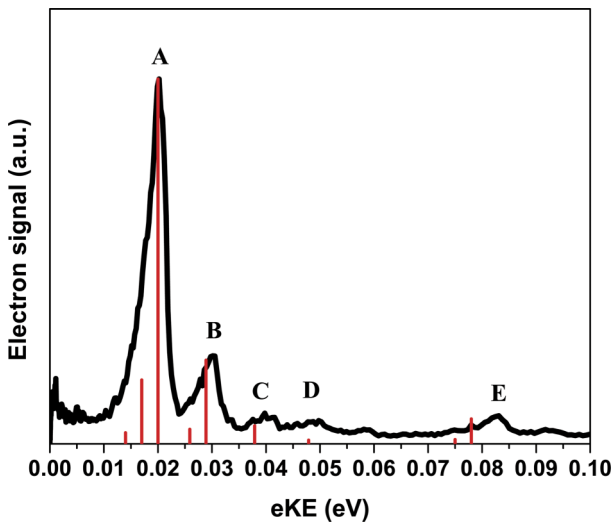

FIG. 2. Anion PES of CH_3SS^- (black) at λ = 698 nm and Franck-Condon simulations at 200 K (red).

TABLE I. Vibrational frequencies (cm^{-1}) of CH_3SS^- and CH_3SS calculated at B3LYP/aug-cc-pVDZ level of theory.

Mode	CH_3SS anion ($\tilde{X}^1A'$)	Neutral ($\tilde{X}^2A''$)
1 (a′)	3069	3146
2	2982	3045
3	1439	1427
4	1275	1298
5	935	946
6	668	665
7	468	580
8	225	249
9 (a″)	3074	3161
10	1403	1419
11	929	913
12	190	118

B. Photofragment mass and translational energy distributions

Figure 3 shows photofragment mass distributions at 248 nm (5.0 eV) and 193 nm (6.4 eV) for CH_3SS and CD_3SS, respectively. Using conservation of momentum, the mass ratio for coincident pairs of photofragments is determined from the scatter distance of the two fragments from the parent beam. This leads to a fragment mass resolution that is mainly dependent on the diameter of the parent beam at the detector which, having a full width at half maximum (FWHM) on the order of 1 mm, yields a fragment mass resolution ($m/\Delta m$) of ~10.

There is evidence for two dissociation channels, but due to the relatively low photofragment mass resolution, the mass spectrum of a single isotopolog is difficult to assign with absolute certainty. Comparing the photodissociation of both CH_3SS and CD_3SS allows better differentiation among possible dissociation channels. The utility of isotopic shifting in assigning mass channels in this experiment has been demonstrated in determining the primary photochemistry of previously studied systems such as C_6H_5S[28] and CH_2CFO.[37]

For CH_3SS at 248 nm, the mass distribution is dominated by two major peaks at approximately 32 and 47 amu corresponding to $S + CH_3S$, $SH + CH_2S$, or some mixture thereof. There is a very small contribution from a mass channel peaking at approximately 15 and 64 amu due to CH_3 and S_2. For CD_3SS, the mass distribution consists of two major peaks at 32 and 50 amu with very low intensity from the 18 and 64 amu mass channel. At 193 nm, the peak positions remain the same, but there is significantly more relative intensity of the 15 and 64 amu and the 18 and 64 amu mass channels for CH_3SS and CD_3SS, respectively.

If SH loss were the major dissociation channel, the corresponding peak in the mass distribution of the deuterated species should shift to higher mass by 1 amu. However, for S loss, this peak position should remain unchanged. As seen in Figure 3, there is no significant shift in the peak at mass 32 amu at either wavelengths, indicating that the contribution from SH (SD) loss is very minor. Furthermore, the translational energy distributions at 248 nm (discussed in Section IV C) are consistent with $CH_3S + S$ being the sole photodissociation products. From here on, the analysis will proceed as considering this channel to be due S atom loss.

Figure 4 shows the corresponding translational energy distribution for the $S + CH_3S$ mass channel at 248 nm. The translational energy distribution appears as one strong peak centered at ~1.25 eV and extending to ~1.6 eV. In addition, the signal for this channel is anisotropic with a measured β parameter of -0.7 ± 0.1, which would correspond to $\beta = 1.4$ for linearly polarized light. The $CH_3 + S_2$ mass channel at this wavelength is too weak to report a reasonable KE distribution.

Figure 5 shows the translational energy distributions for the two mass channels at 193 nm. The distribution for S loss is quite different from what is observed at 248 nm; it is very broad, extending from zero to the maximal available energy of ~2.8 eV. For the $CH_3 + S_2$ mass channel, the translational energy distribution is bimodal with the low-energy feature extending from zero to ~1.75 eV, while the higher-energy feature spans ~2–3.5 eV. The angular distributions for both channels are isotropic within the experimental accuracy. The vertical lines in Fig. 5 correspond to the maximal allowed E_T

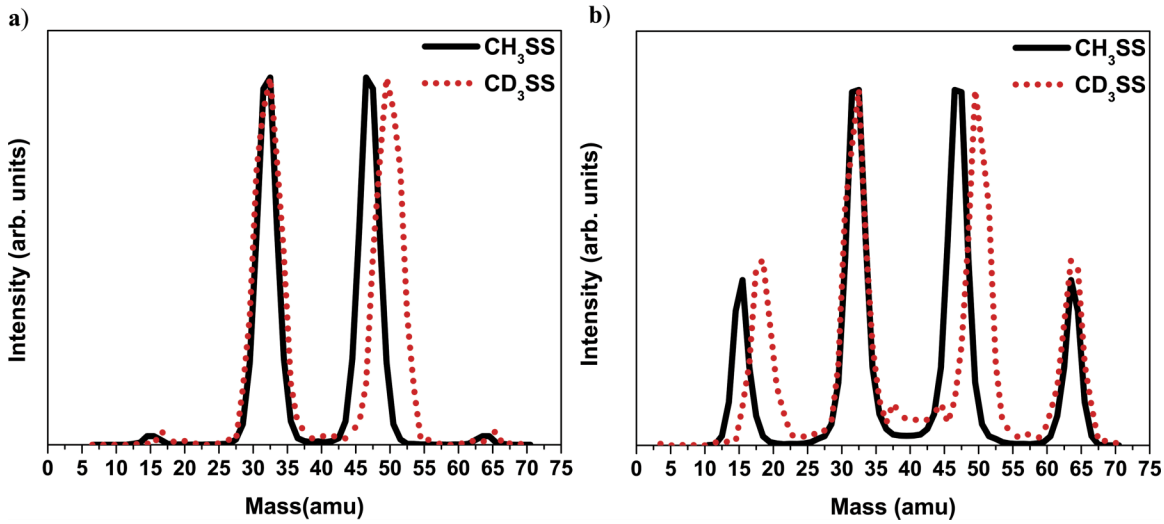

FIG. 3. Photofragment mass distributions at (a) 248 nm and (b) 193 nm for CH_3SS (solid, black) and CD_3SS (dotted, red), respectively.

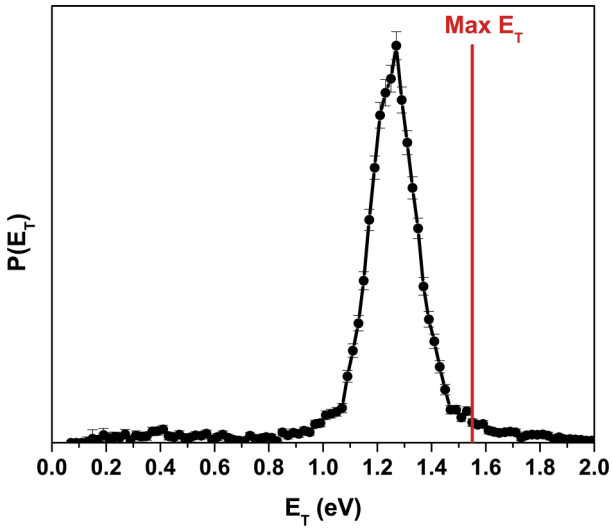

FIG. 4. Translational energy distribution for S loss at 248 nm. Vertical line (red) indicates the calculated maximum available energy for S loss.

for various product electronic states and are discussed in more detail in Section IV.

IV. ANALYSIS AND DISCUSSION

A. Anion photoelectron spectrum

There are several features present in the anion photoelectron spectrum labelled A-E. Peak A at eKE = 0.020 eV, the most intense peak in the spectrum, is assigned to the transition from the vibrational ground state of the anion to the vibrational ground state of the neutral radical (0_0^0). At the detachment wavelength of 698 nm (1.777 eV), this gives an EA for CH_3SS of 1.757 eV in exact agreement with the value measured by Moran and Ellison.[9] It should be noted that the previously reported spectrum at a detachment energy of 2.540 eV looks quite different than the one presented here. In a standard photoelectron spectrum, photodetachment is typically performed well above the EA in order to observe the entire Franck-Condon profile and to mitigate cross-sectional effects associated with near-threshold detachment. The PES in Figure 2, in contrast, provides the vibrational distribution of the radical prior to dissociation in our experiment.

TABLE II. Peak positions, shifts from origin, and assignments for anion PES of CH_3SS^- (Fig. 2).

Peak	Position (eV)	Shift from origin (cm^{-1})	Assignment
A	0.020	0	0_0^0
B	0.030	81	12_1^1
C	0.039	153	12_2^2
D	0.049	234	8_1^0
E	0.083	508	7_1^0

We performed FC simulations using the calculated vibrational frequencies shown in Table I. Anion and neutral structures were optimized followed by frequency calculations with density functional theory (DFT) using the B3LYP functional and the Dunning-type cc-pVDZ basis set augmented with diffuse functions using Gaussian 09.[38] Overlap integrals are calculated in the harmonic oscillator approximation, including mixing of the neutral vibrational modes via Duschinsky rotation.

As shown in Figure 2 in red, the FC simulation at a vibrational temperature of 200 K matches well with the experimentally measured spectrum at λ = 698 nm. Using these simulations, peaks B-E could be assigned as indicated in Table II.

Peak B, the second most intense feature, occurs at approximately 0.01 eV higher eKE than peak A. This separation (~80 cm^{-1}) is too small to be a hot band (Table II). Instead, this peak can be assigned to a sequence band in the lowest-frequency torsional mode of CH_3SS (12_1^1), with peak C corresponding to the next band in this sequence (12_2^2). The additional features in the spectrum, D and E, arise from transitions to the vibrational ground state of the neutral radical from one quantum of vibrational excitation in the anion

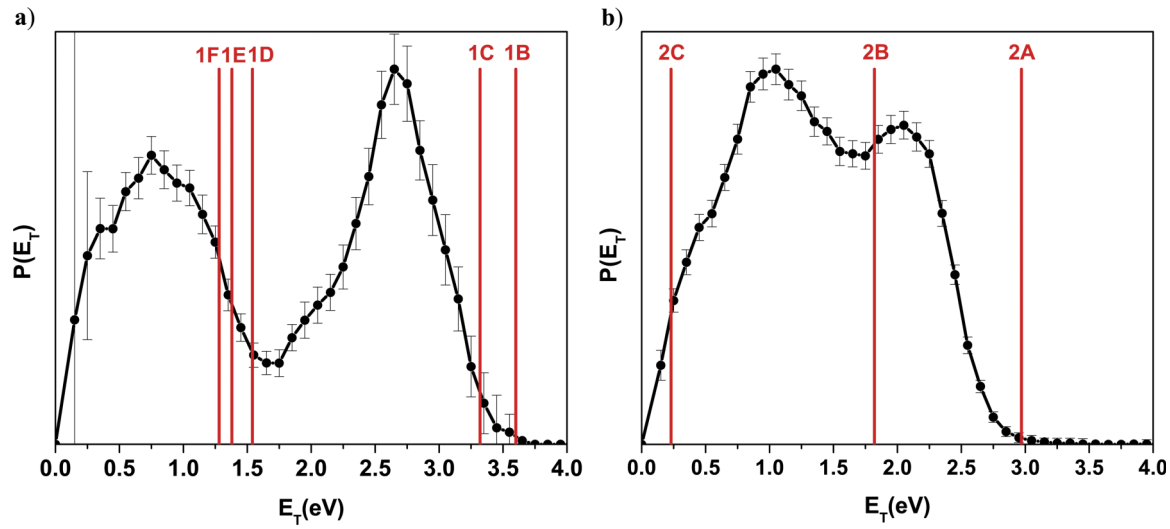

FIG. 5. Translational energy distributions for (a) $CH_3 + S_2$ and (b) $CH_3S + S$ mass channels at 193 nm. Vertical lines (red) indicate the calculated maximum available energy for possible product states (Table IV).

TABLE III. Product branching fractions at each dissociation wavelength.

Wavelength (nm)	$CH_3S + S$ (%)	$CH_3 + S_2$ (%)
248	96	4
193	68	32

C–S–S bending and S–S stretching modes, respectively. These hot bands provide a direct measurement of the vibrational frequencies in the anion of ~233 cm^{-1} for the bending mode and ~508 cm^{-1} for the stretch. There is some discrepancy between calculated and measured values of S–S stretching frequency of the anion (Tables I and II), with the calculation underestimating this frequency by ~40 cm^{-1}.

There are also two additional peaks in the FC simulation that occur at lower eKE than the vibrational origin (peak A) that corresponds to the 8_1^1 and 8_2^2 transitions. As peak A appears to be broadened towards low kinetic energy, there could be some contribution from these transitions to the experimental spectrum. Finally, the last two features present on the FC simulation that do not have assignments in the experimental spectrum are the $8_1^1 12_1^1$ (~0.026 eV) and $7_1^0 8_1^1$ (~0.075 eV) combination bands.

B. Product branching fractions

The branching fractions for each product channel are shown in Table III. At 248 nm, the mass distributions show that the products formed are almost exclusively the methylthio radical (CH_3S) and sulfur atom with virtually no population of the $S_2 + CH_3$ radical dissociation channel. The measured branching fraction at 248 nm is consistent with the value determined in the re-investigation of methyl perthiyl with our molecular beam instrument (94%).[18] At 193 nm, the branching ratios change substantially. While S loss remains the dominant channel (68%), S_2 loss is much more prevalent than at 248 nm and constitutes nearly a third of the total photofragmentation. We estimate the uncertainty in the measurements to be ±1%.

C. Photodissociation dynamics

1. 248 nm

From energy conservation, the translational energy release of the photofragments, E_T, is given by the following relationship:

$$E_T = h\nu - E_{int} - D_0, \quad (6)$$

where $h\nu$ is the photon energy, E_{int} is the internal energy of fragments, and D_0 is the bond dissociation energy. Eq. (6) assumes that the precursor radicals have no internal energy, although the anion photoelectron spectrum shows that there is a small population of vibrationally excited radicals (Section IV A).

As shown in Figure 4, the translational energy distribution for the S loss channel at 248 nm (5.0 eV) is sharply peaked near the maximal available energy for this dissociation channel (with zero internal energy in CH_3SS) as calculated from previously reported heats of formation.[10,14,16] This result indicates that the dissociation occurs on an excited state that is repulsive with respect to S atom loss, leading to ground-state products: $CH_3S(\tilde{X}^2E) + S(^3P)$. A repulsive dissociation is consistent with the anisotropic photofragment angular distribution with an anisotropy parameter $\beta \approx 1.4$. This value indicates a transition dipole moment that is nearly parallel to the S–S bond axis. As was also seen in the molecular beam study,[18] the peak of the translational energy distribution lies around 0.25 eV below the maximum allowed energy. The S–S–C bond angle in CH_3SS is calculated to be ~106°, so this energy gap most likely arises from rotational excitation of the CH_3S fragment as the radical dissociates repulsively.

These results also provide a direct comparison to the photodissociation of DMDS at 248 nm reported by Lee and co-workers.[6] In that study, they found that absorption resulted in exclusive S–S bond cleavage, leading to two CH_3S fragments with the maximal available translational energy. They also found an anisotropy parameter of $\beta \approx 1.2$, very close to the value of 1.4 measured here. The photodissociation dynamics were attributed to a $\sigma^*_{ss} \leftarrow n_s$ transition in the S–S moiety of the molecule. These results suggest that the photochemistry at 248 nm of DMDS and methyl perthiyl is very similar.

Previous theoretical study on the low-lying excited states of CH_3SS[13] found that the transition to the $\tilde{B}^2A''$ state at a vertical excitation energy of approximately 3.4 eV has strong oscillator strength. This state is analogous to the $\tilde{B}$-state of the methyl peroxy radical (CH_3OO) which is known to be repulsive with respect to the O–O bond coordinate.[39] It is possible that this state contributes to the photodissociation dynamics of CH_3SS at 248 nm (5 eV) resulting in repulsive S atom dissociation, but the photon energy is substantially higher than the calculated vertical excitation energy, making this assignment uncertain.

2. 193 nm

At 193 nm, the photodissociation dynamics of CH_3SS are very different from what is observed at 248 nm. There is significantly more population of the S_2 loss channel, and the translational energy distributions are more complicated, making it necessary to provide a more thorough overview of the possible excited electronic states available to the products. The energetics are outlined in Table IV with values obtained

TABLE IV. Energetically allowed dissociation channels of CH_3SS at λ = 193 nm (6.4 eV). All energies are in eV.

Mass channel	Product channel	D_o	Max E_T at	Label
15 + 64	$CH_3(\tilde{X}^2A_2'') + S_2(X^3\Sigma_g^-)$	2.11	4.29	1A
	$CH_3(\tilde{X}^2A_2'') + S_2(a^1\Delta_g)$	2.82	3.58	1B
	$CH_3(\tilde{X}^2A_2'') + S_2(b^1\Sigma_g^+)$	3.10	3.30	1C
	$CH_3(\tilde{X}^2A_2'') + S_2(c^1\Sigma_u^-)$	4.88	1.52	1D
	$CH_3(\tilde{X}^2A_2'') + S_2(A'^3\Delta_u)$	5.04	1.36	1E
	$CH_3(\tilde{X}^2A_2'') + S_2(A^3\Sigma_u^+)$	5.14	1.26	1F
32 + 47	$CH_3S(\tilde{X}^2E) + S(^3P)$	3.45	2.95	2A
	$CH_3S(\tilde{X}^2E) + S(^1D)$	4.60	1.80	2B
	$CH_3S(\tilde{X}^2E) + S(^1S)$	6.19	0.21	2C

from both experimental and theoretical sources.[10,14–16,40] None of the excited electronic states of the methyl (CH_3) or methylthio (CH_3S) radicals are accessible at 193 nm, so the different possible products states in Table IV are due to various excited states of either the S_2 or S atom fragment.

For S_2 loss, the translational energy distribution is bimodal. Furthermore, it does not extend out to the maximal available energy for ground-state products but instead ends near the maximum E_T for channel 1B. Hence, this feature is likely due to the production of S_2 in its lowest-lying singlet state ($a^1\Delta_g$). There could also be some contribution from channel 1C, with S_2 in the $b^1\Sigma_g^+$ state, for which the maximum E_T is 3.32 eV. The lower-energy feature ends near the max E_T for channel 1D; however, both channels 1E and 1F would be in approximately the same energy range and could very well contribute to the intensity in this energy range. It thus appears that S_2 excited state production dominates at 193 nm.

For S loss, we find that the translational energy distribution ends near the maximal available energy at 193 nm of approximately 3 eV for ground-state products. This distribution is consistent with dissociation involving repulsive excited states, as was observed at 248 nm. In contrast to the results at 248 nm, the distribution is broad with hints of structure and extends to zero translational energy, suggesting contributions from higher-lying product channels. The other energetically allowed dissociation channels at this wavelength involve the production of sulfur atom in its excited ^1D and ^1S states, although the ^1S pathway (2C) can only contribute at very low translational energies (<0.2 eV). There appear to be two major features in the energy distribution peaking near 2.0 and 1.0 eV that likely correspond to channels 2A and 2B, respectively. It is clear from the width of these features that the CH_3S fragment is formed with a large spread of internal (vibrational and rotational) energy.

To our knowledge, the excited electronic states of CH_3SS at the photodissociation wavelengths used here are not well characterized. Our results suggest that at both wavelengths, either a repulsive state is accessed directly or a bound excited state undergoes predissociation via a repulsive state. Further theoretical study on the excited state spectroscopy and dynamics of this radical at higher excitation energies would be exceedingly useful in sorting out these possible dissociation mechanisms.

V. CONCLUSIONS

We have studied the photodissociation dynamics of methyl perthiyl at 248 and 193 nm by means of fast-beam coincidence translational spectroscopy. Our experiment yields the primary photochemistry for methyl perthiyl photodissociation, including the product branching ratios and translational energy distributions. S atom loss channel was identified as the dominant dissociation channel at 248 nm, with almost no population of the S_2 loss channel. The translational energy distribution at 248 nm peaks near the maximal allowed energy, indicating dissociation on an excited-state repulsive potential energy surface. These results are consistent with the most recent results obtained with the molecular-beam photodissociation instrument in our research group.[18] At 193 nm, S_2 loss becomes more prominent (32%), with S atom loss still being the major dissociation channel. The translational energy distributions for both channels are very broad and bimodal, suggesting that the S and S_2 fragments are formed in multiple electronic states.

ACKNOWLEDGMENTS

The authors would like to thank Dr. Neil-Cole Filipiak and Mark Shapero for their help in completing this work. This research was supported by the Director, Office of Basic Energy Science, Chemical Sciences Division of the U.S. Department of Energy under Contract No. DE-AC02-05CH11231.

[1]W. J. Wedemeyer, E. Welker, M. Narayan, and H. A. Scheraga, Biochemistry **39**, 4207 (2000).
[2]T. E. Graedel, Rev. Geophys. **15**, 421, doi:10.1029/RG015i004p00421 (1977).
[3]V. P. Aneja, A. P. Aneja, and D. F. Adams, J. Air Pollut. Control Assoc. **32**, 803 (1982).
[4]P. D. Lightfoot, R. A. Cox, J. N. Crowley, M. Destriau, G. D. Hayman, M. E. Jenkin, G. K. Moortgat, and F. Zabel, Atmos. Environ., Part A **26**, 1805 (1992).
[5]A. B. Callear and D. R. Dickson, Trans. Faraday Soc. **66**, 1987 (1970).
[6]Y. R. Lee, C. L. Chiu, and S. M. Lin, J. Chem. Phys. **100**, 7376 (1994).
[7]B. Martínez-Haya, M. J. Bass, M. Brouard, C. Vallance, I. Torres, and J. Barr, J. Chem. Phys. **120**, 11042 (2004).
[8]S. Nourbakhsh, C. L. Liao, and C. Y. Ng, J. Chem. Phys. **92**, 6587 (1990).
[9]S. Moran and G. B. Ellison, J. Phys. Chem. **92**, 1794 (1988).
[10]Z. X. Ma, C. L. Liao, C. Y. Ng, Y. S. Cheung, W. K. Li, and T. Baer, J. Chem. Phys. **100**, 4870 (1994).
[11]G. Maofa, W. Jing, S. Zheng, Z. Xinjiang, and W. Dianxun, J. Chem. Phys. **114**, 3051 (2001).
[12]Y. Cheung, W. Li, and C. Ng, J. Mol. Struct.: THEOCHEM **339**, 25 (1995).
[13]M.-X. Song, Z.-X. Zhao, W. Zhang, F.-Q. Bai, H.-X. Zhang, and C.-C. Sun, Int. J. Quantum Chem. **112**, 1537 (2012).
[14]R. T. Bise, H. Choi, H. B. Pedersen, D. H. Mordaunt, and D. M. Neumark, J. Chem. Phys. **110**, 805 (1999).
[15]M. W. Chase, Jr., *NIST-JANAF Thermochemical Tables*, 4th ed. (NIST, Gaithersberg, MD, 1998), pp. 1–1951.
[16]B. Nagy, P. Szakács, J. Csontos, Z. Rolik, G. Tasi, and M. Kállay, J. Phys. Chem. A **115**, 7823 (2011).
[17]N. C. Cole-Filipiak, B. Negru, G. M. P. Just, D. Park, and D. M. Neumark, J. Chem. Phys. **138**, 054301 (2013).
[18]N. C. Cole-Filipiak, M. Shapero, C. Haibach-Morris, and D. M. Neumark, "Production and photodissociation of the methyl perthiyl radical," J. Phys. Chem. A (published online 2016).
[19]R. E. Continetti, D. R. Cyr, D. L. Osborn, D. J. Leahy, and D. M. Neumark, J. Chem. Phys. **99**, 2616 (1993).
[20]R. E. Continetti, D. R. Cyr, R. B. Metz, and D. M. Neumark, Chem. Phys. Lett. **182**, 406 (1991).
[21]A. A. Hoops, J. R. Gascooke, A. E. Faulhaber, K. E. Kautzman, and D. M. Neumark, Chem. Phys. Lett. **374**, 235 (2003).
[22]E. Garand, T. I. Yacovitch, and D. M. Neumark, J. Chem. Phys. **130**, 064304 (2009).
[23]J. M. B. Bakker, J. Phys. E **6**, 785 (1973).
[24]J. M. B. Bakker, J. Phys. E **7**, 364 (1974).
[25]O. Jagutzki, A. Cerezo, A. Czasch, R. Dorner, M. Hattas, H. Min, V. Mergel, U. Spillmann, K. Ullmann-Pfleger, T. Weber, H. Schmidt-Bocking, and G. D. W. Smith, IEEE Trans. Nucl. Sci. **49**, 2477 (2002).
[26]M. Lampton, O. Siegmund, and R. Raffanti, Rev. Sci. Instrum. **58**, 2298 (1987).
[27]K. A. Hanold, A. K. Luong, T. G. Clements, and R. E. Continetti, Rev. Sci. Instrum. **70**, 2268 (1999).
[28]A. W. Harrison, J. S. Lim, M. Ryazanov, G. Wang, S. Gao, and D. M. Neumark, J. Phys. Chem. A **117**, 11970 (2013).
[29]M. Ryazanov, A. W. Harrison, G. Wang, P. E. Crider, and D. M. Neumark, J. Chem. Phys. **140**, 234304 (2014).
[30]D. J. Leahy, D. L. Osborn, D. R. Cyr, and D. M. Neumark, J. Chem. Phys. **103**, 2495 (1995).

[31]R. N. Zare, Mol. Photochem. **4**, 1 (1972).
[32]See supplementary material at http://dx.doi.org/10.1063/1.4955195 for schematics and further description of the velocity-map imaging photoelectron spectrometer.
[33]M. Ryazanov and H. Reisler, J. Chem. Phys. **138**, 144201 (2013).
[34]S. J. Cavanagh, S. T. Gibson, and B. R. Lewis, J. Chem. Phys. **137**, 144304 (2012).
[35]S. J. Cavanagh, S. T. Gibson, M. N. Gale, C. J. Dedman, E. H. Roberts, and B. R. Lewis, Phys. Rev. A **76**, 052708 (2007).
[36]V. A. Mozhayskiy and A. I. Krylov, ezSpectrum, 2009, http://iopenshell.usc.edu/downloads.
[37]A. A. Hoops, J. R. Gascooke, K. E. Kautzman, A. E. Faulhaber, and D. M. Neumark, J. Chem. Phys. **120**, 8494 (2004).
[38]M. J. Frisch, G. W. Trucks, H. B. Schlegel, G. E. Scuseria, M. A. Robb, J. R. Cheeseman, G. Scalmani, V. Barone, B. Mennucci, G. A. Petersson, H. Nakatsuji, M. Caricato, X. Li, H. P. Hratchian, A. F. Izmaylov, J. Bloino, G. Zheng, J. L. Sonnenberg, M. Hada, M. Ehara, K. Toyota, R. Fukuda, J. Hasegawa, M. Ishida, T. Nakajima, Y. Honda, O. Kitao, H. Nakai, T. Vreven, J. A. Montgomery, J. E. Peralta, F. Ogliaro, M. Bearpark, J. J. Heyd, E. Brothers, K. N. Kudin, V. N. Staroverov, R. Kobayashi, J. Normand, K. Raghavachari, A. Rendell, J. C. Burant, S. S. Iyengar, J. Tomasi, M. Cossi, N. Rega, J. M. Millam, M. Klene, J. E. Knox, J. B. Cross, V. Bakken, C. Adamo, J. Jaramillo, R. Gomperts, R. E. Stratmann, O. Yazyev, A. J. Austin, R. Cammi, C. Pomelli, J. W. Ochterski, R. L. Martin, K. Morokuma, V. G. Zakrzewski, G. A. Voth, P. Salvador, J. J. Dannenberg, S. Dapprich, A. D. Daniels, Ö. Farkas, J. B. Foresman, J. V. Ortiz, J. Cioslowski, and D. J. Fox, GAUSSIAN 09, Revision B.01, Gaussian, Inc., 2009.
[39]J. A. Jafri and D. H. Phillips, J. Am. Chem. Soc. **112**, 2586 (1990).
[40]M. Tashiro, Chem. Phys. Lett. **453**, 145 (2008).